Environ Monit Assess (2018) 190: 188
https://doi.org/10.1007/s10661-018-6565-y

# Feasibility of applying the LED-UV-induced $TiO_2$/ZnO-supported $H_3PMo_{12}O_{40}$ nanoparticles in photocatalytic degradation of aniline

**Mahmoud Taghavi · Mohammad Taghi Ghaneian · Mohammad Hasan Ehrampoush · Masoumeh Tabatabaee · Mojtaba Afsharnia · Ali Alami · Jalal Mardaneh**

Received: 4 November 2017 / Accepted: 19 February 2018 / Published online: 3 March 2018


**Abstract** In the present study, $TiO_2$/ZnO-supported phosphomolybdic acid nanoparticles are investigated by the impregnation method, followed by analyzing their photocatalytic activity under UV-LED light and degradation kinetics degrading aniline as an organic pollutant model. Nanoparticle characteristics and the remaining Keggin structure in the nanocomposites were confirmed by means of FESEM, FTIR, and XRD analyses. Heterogenization of phosphomolybdic acid on $TiO_2$ and ZnO nanoparticles resulted in the improved light absorption intensity and decreased band gap of nanocomposites. Photocatalytic degradation of aniline was also improved for composite nanoparticles and reached to 25.62, 43.48, and 38.25% for $TiO_2$/HPMo, ZnO/HPMo, and $TiO_2$/ZnO/HPMo, respectively. Overall, the results showed a good fit to the Langmuir-Hinshelwood kinetic model.

**Keywords** Polyoxometalate · Phosphomolybdic acid · Photocatalytic degradation · Aniline · $TiO_2$ · ZnO

M. Taghavi · M. T. Ghaneian · M. H. Ehrampoush
Environmental Science and Technology Research Center, Department of Environmental Health Engineering, Shahid Sadoughi University of Medical Sciences, Yazd, Iran

M. Taghavi · M. Afsharnia
Department of Environmental Health Engineering, School of Public Health, Social Development & Health Promotion Research Center, Gonabad University of Medical Sciences, Gonabad, Iran

M. Tabatabaee (✉)
Department of Chemistry, Yazd Branch, Islamic Azad University, Yazd, Iran
e-mail: tabatabaee@iauyazd.ac.ir

A. Alami
Social Determinants of Health Research Center; Department of Social Medicine, School of Medicine, Gonabad University of Medical Sciences, Gonabad, Iran

J. Mardaneh
Department of Microbiology, School of Medicine, Gonabad University of Medical Sciences, Gonabad, Iran

## Introduction

Water pollution with organic pollutants is one of the main concerns regarding the pollution prevention of water resources due to the shortage of water resources, growing population, and increasing water demand (Zabihi-Mobarakeh and Nezamzadeh-Ejhieh 2015; Samarghandy et al. 2011; Khosravi et al. 2017; Eslami et al. 2018). Aniline and its derivatives are frequently found in wastewater of rubber, dye, pharmaceutical, and pesticide and herbicide industries. This pollution can occur through using aniline in their industrial manufacture or as a result of the biodegradation of xenobiotic compounds (Szczepanik and Słomkiewicz 2016). Aniline is refractory to biodegradation and is toxic to humans and the aquatic life. This pollutant will find its way to reach the water resources. So, water and industrial wastewater containing aniline demand a treatment process before discharging to the environment (Orge et al. 2016). Among various technologies for removal of organic pollutants, photocatalytic degradation has attracted growing attention due to its

benefits (Szczepanik and Słomkiewicz 2016; Anotai et al. 2012; Ku et al. 2010). This technology takes advantage of a light source to generate electron-hole pairs and reactive species, which are responsible for pollutant degradation (Taghi Ghaneian et al. 2016; Taghavi et al. 2018). However, the old light sources such as mercury vapor lamps in this technology have some drawback including instability of power during operation, high voltage needed at the initial stage, heat generation, required cooling system, low lifetime, use of hazardous metal, low photonic efficiency, and a broader spectral wavelength. The use of solar light, on the other hand, has its own disadvantages such as high cost, need a larger area for installation, dependence to reactors efficiency on direction, and availability of solar light (Natarajan et al. 2011). Application of ultraviolet light emitting diodes (UV-LEDs) is a solution for overcoming the above-mentioned limitations (Jamali et al. 2013). However, there is a need to investigate the applicability of this light source for degradation of various pollutants using different photocatalysts. Application of heteropoly acids in combination with semiconductors in photocatalytic degradation has reported by some researchers. Lei et al. (Xu et al. 2012) reported degradation of sulfamethoxazole over the metallic silver and Keggin unit codoped titania nanocomposites up to 97.8% after 90 min irradiation by Xe lamp. A degradation efficiency of 97.7% for rhodamine B with $H_3PW_{12}O_{40}/SiO_2$ has also reported by Yang et al. (2012). Furthermore, degradation of phenol and triethyl phosphate (Li et al. 2015), dinitrotoluene (Feng et al. 2014), bisphenol A (Lu et al. 2013), and nitrobenzene (Wang et al. 2010) by $H_3PW_{12}O_{40}/TiO_2$, methyl orange by $H_3PW_{12}O_{40}$/activated clay (Wei et al. 2012), and atrazine by $H_3PW_{12}O_{40}$/Ag-$TiO_2$ (Xu et al. 2013) was reported in other studies.

In the present work, we report the synthesis of $TiO_2$ and ZnO-supported phosphomolybdic acid nanoparticles ($TiO_2$/PMA, ZnO/PMA, and $TiO_2$/ZnO/PMA) by impregnation method and investigate their photocatalytic activity under UV-LED light and degradation kinetics degrading aniline as an organic pollutant model.

## Materials and methods

All chemicals used in this study were provided by the Merck Company in synthesis grade. Distilled water was used for the preparation of the synthetic solution. The flowchart of the experimental process was shown in Fig. 1.

### Nanoparticle preparation

To synthesize $TiO_2$ nanoparticle, 3.4 mL tetra-n-butyl titanate was added to 10 mL ethanol. Next, 4 mL acetic acid and distilled water 1:1 (*v*/*v*) were added dropwise to this solution and the reaction mixture was stirred at 25 °C for 2 h. Then, the gel was dried at 100 °C and calcinated at 500 °C for 3 h.

ZnO nanoparticles were synthesized by dissolving 5 mM zinc acetate dihydrate and 7.5 mM sodium tartrate in 50 mL distilled water. After 30 min, the pH of the solution was reached 10 using ammonia. The solution was refluxed for 6 h. Then, solids were separated and dried at 80 °C in the oven. Calcination was performed at 600 °C for 2 h.

$TiO_2$/ZnO nanoparticle was prepared by dissolving 3.4 mL titanium butoxide in a mixture of ethanol (6 mL) and distilled water (1 mL). Then, the pH of the solution was adjusted to 2 using hydrochloric acid (solution 1). After that, 0.2 mM SDS sodium dodecyl sulfate was

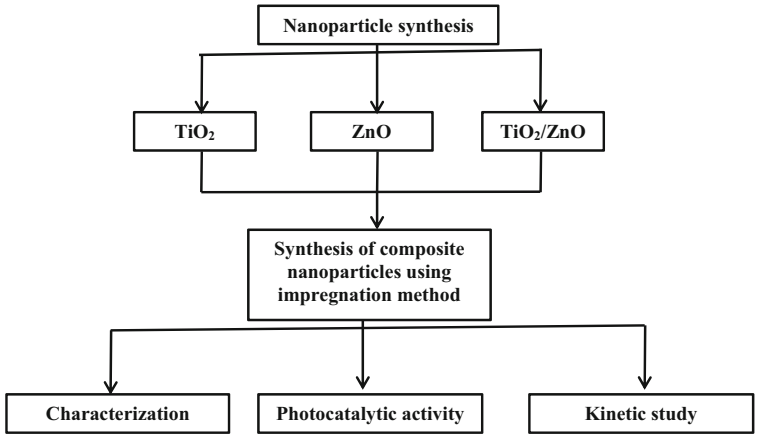


**Fig. 1** The flowchart of the experimental process

dissolved in 4 mL ethanol and then added dropwise to solution 1 at a flow rate of 0.5 mL/min approximately. In the next step, 0.34 g zinc nitrate hexahydrate was dissolved in 5 mL distilled water and was added slowly to the obtained solution. The reaction mixture was kept at room temperature for 2 h. The prepared gel was dried in an oven at 70 °C and calcinated at 700 °C for 2 h.

$TiO_2$/HPMo nanoparticles were obtained using impregnation method, described below. First, 6 g $TiO_2$ nanoparticle was dispersed in 100 mL distilled water. Then, 2 g phosphomolybdic acid (HPMo) was added to the mixture. The reaction mixture was placed in a Parr-Teflon lined stainless steel vessel, sealed, and heated at 150 °C for 3 h. Next, the suspension was placed on a hotplate until it completely evaporated. Likewise, ZnO/HPMo and $TiO_2$/ZnO/HPMo nanoparticles were also prepared.

## Nanoparticle characterization

The surface morphology of the nanoparticles was specified using a field emission scanning electron microscopy (FESEM, TE-SCAN microscope, MIRA3, Czech Republic) with an acceleration voltage of 15 kV.

Phase analysis and crystalline structure of the nanoparticles were characterized using X-ray diffraction (XRD, Philips, PW1730) equipped with Cu-K$\alpha$ radiation ($\lambda = 1.5406$ Å) scanned for $2\theta$ between 10° and 80° (step size 0.05°, scan step time 1 s). To determine crystalline structures, the distances between peaks were compared with the JCDPS no. 21-1272, 21-1275, and 5-0664 of the International Center for Diffraction Data.

The crystallite size was calculated from the broadening of peaks using Scherer's formula.

$$D = \frac{k\lambda}{\beta\cos\theta} \tag{1}$$

where $D$ and $K$ are the crystallite size (nm) and the shape constant (0.9), respectively, $\lambda$ parameter is the wavelength of Cu, K$\alpha$ radiation (1.5406 A°), $\theta$ is the diffraction angle (°), and $\beta$ the full width at half maximum (Leong et al. 2014).

Surface structure and the functional groups on the surface of all samples were characterized using Fourier transform infrared (FT-IR) spectroscopy. The IR spectra of the nanoparticles were analyzed using an FT-IR spectrometer with pressed pellets made using KBr powder as a diluent in the wave number in the range of 400–4000 $cm^{-1}$.

Optical properties of nanoparticles were evaluated using diffuse reflection spectroscopy (DRS) in a range of 300–700 nm. The UV-Vis reflectance spectra were measured with Avantes spectrophotometer (AvaSpec-ULS2048LTEC).

The Kubelka-Munk function was used to evaluate the band gap of nanoparticles. This function indicates the ratio of the absorption coefficient and scattering coefficient based on the following equation:

$$F(R) = \frac{\alpha}{S} = \frac{(1-R)^2}{2R} \tag{2}$$

where $\alpha$ and $S$ indicate absorption coefficient and scattering coefficient, respectively and $R$ is reflectance. Assuming $S$ to be constant, which is generally reasonable around band edge, $F(R)$ would be proportional to the absorption coefficient ($\alpha$) (Toyoura et al. 2005).

For band gap calculation, the fundamental equation is used as follows:

$$F(R)(h\nu) \approx B\left(h\nu - E_g\right)^n \tag{3}$$

where $E_g$ is the band gap (eV) of semiconductor, $h$ is Planck's constant (J.s), $B$ is the absorption constant, and $\nu$ is the light frequency ($s^{-1}$) (López and Gómez 2012; Toyoura et al. 2005; Kumari et al. 2015). For an indirect-allowed transition, $n$ is equal 2 and for a direct-allowed transition, $n$ is equal to $\frac{1}{2}$. So, the band gap can be estimated from plotted $F(R)(h\nu)^{1/2}$ for an indirect-allowed transition or $F(R)(h\nu)^2$ for a direct-allowed transition versus $h\nu$. The line drawn on the linear part of the plot gives the band gap (Choudhury et al. 2013).

## Photocatalytic assessment

Photocatalytic experiments were performed in a reactor consisting of a cylindrical quartz chamber with a source light around the chamber. The reactor and stirrer were placed in a box equipped with a fan on top and some holes at the bottom for cooling the reactor and source light. Inside the box was a thin layer of aluminum foil with a purity of 99%. The light was supplied using 42 LED lamps (3.2 V, $\lambda = 390$ nm) installed on the inner wall of a cylinder, which surrounds the reactor. The LED reactor used in photocatalytic experiments is presented in Fig. 2. A 100-mL solution containing 50 mg/L of aniline without pH adjustment was prepared and

0.05 g nanoparticle was added to the solution. Five millimolars per liter hydrogen peroxide as electron scavenger was also added to the solution. In each run, the solution was magnetically stirred in the dark for 30 min before the irradiation to ensure adsorption-desorption equilibrium. At given time intervals, 2 mL of the solution was taken out and the nanoparticle was removed through centrifuging at 13000 rpm for 30 min. The final concentration of aniline in the supernatant was determined using the spectrophotometric method at 555 nm using N-(1-naphthyl) ethylenediamine according to previous researchs (Norwitz and Keliher 1981; Sarwade and Gawai 2014; Sun et al. 2015). This method has introduced by Norwitz et al. (Norwitz and Keliher 1981) and its details can be found in their study. A limitation of the present study is that samples were not analyzed by other detection methods.

The degradation efficiency of aniline was calculated through the following equation:

$$\text{Degradation efficiency}(\%) = \frac{(C_0 - C_t)}{C_0} \times 100 \qquad (4)$$

where $C_0$ and $C_t$ are aniline concentration at initial and time of $t$.

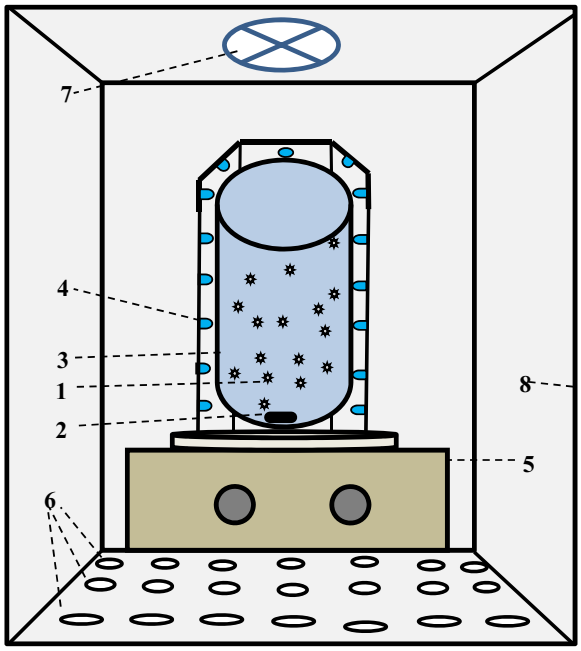


**Fig. 2** LED reactor used in photocatalytic experiments. 1: Nanocomposite, 2: Magnet, 3: Quartz chamber, 4: Transect of source light (LED), 5: Stirrer, 6: Holes, 7: Fan, 8: Box covered with a thin layer of aluminum foil

The tests were performed in triplicate and the data were presented as their mean. Data were analyzed using repeated measures ANOVA at a significant level of 0.05, and LSD post hoc test was done when a significant difference was observed in the ANOVA test.

### Photocatalytic degradation kinetic

The photocatalytic degradation of aniline by nanoparticles was fitted by the Langmuir-Hinshelwood, which can be presented by the following equation:

$$Ln\frac{C_0}{C} = kt \qquad (5)$$

where $C_0$ and $C$ are initial and final concentrations of aniline, respectively and $k$ is the rate constant that can be obtained from the slope of the straight-line of the plot of $Ln(C/C_0)$ versus $t$ as a function of the used experimental parameters (Kuvarega et al. 2015; Zabihi-Mobarakeh and Nezamzadeh-Ejhieh 2015).

## Results and discussion

### Nanoparticle characterization

#### *Morphology*

Using the FESEM measurements of the nanoparticles (Fig. 3), $TiO_2$/HPMo and $TiO_2$/ZnO/HPMo show a spherical shape with relatively uniform particle size ranging from 78 to 112 nm and 28 to 38 nm, respectively, where a slight particle aggregation also occurs. However, ZnO/HPMo nanoparticles showed round particle and some sheet-like aggregation with particle size ranging from 13 to 48 nm.

#### *Phase analysis and crystal structure*

The XRD patterns of the synthesized nanoparticles are presented in Fig. 4. The diffraction peaks obtained fit well with the ICSD demonstrating the tetragonal anatase phase of $TiO_2$ in $TiO_2$/HPMo nanoparticles. ZnO in ZnO/HPMo nanoparticles is crystalline in nature and the diffraction peaks match well with a hexagonal zincite phase. XRD pattern of $TiO_2$/ZnO/HPMo nanoparticles indicates the rutile phase for $TiO_2$ and zincite phase for ZnO.

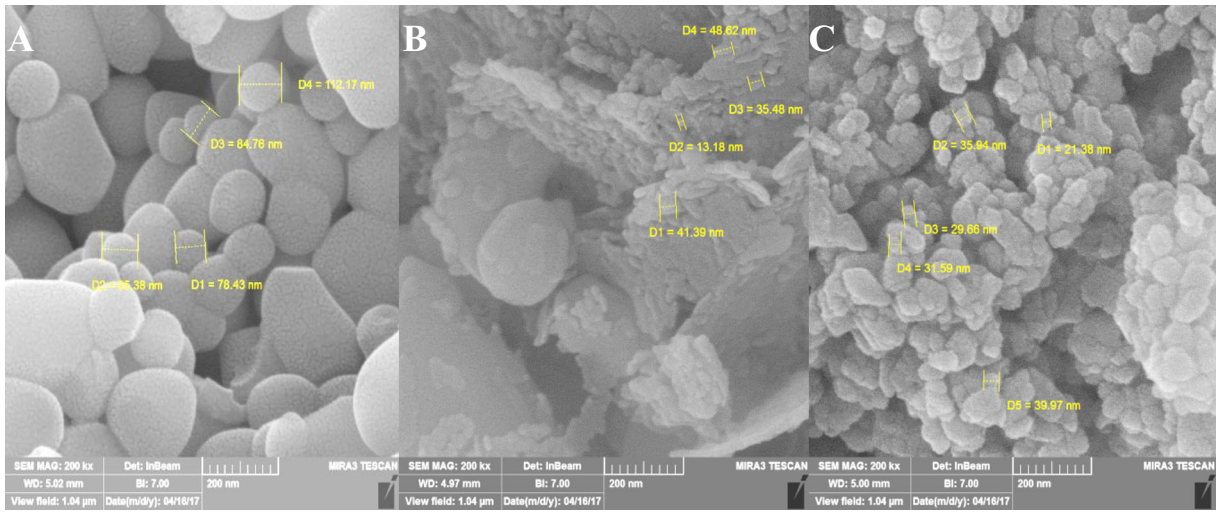


**Fig. 3** The field emission scanning electron micrographs (FESEM) of the $TiO_2$/HPMo (**a**), ZnO/HPMo (**b**), and $TiO_2$/ZnO/HPMo (**c**) nanoparticles

The crystallite size of nanoparticles obtained from the broadening of peaks using Scherer's formula was found to be 45, 28, and 23 nm for $TiO_2$/HPMo, ZnO/HPMo, and $TiO_2$/ZnO/HPMo, respectively.

*Surface structure*

The FT-IR absorption spectrum of nanoparticles is shown in Fig. 5. The peaks at 1062 and 962 $cm^{-1}$ in the absorption spectrum of $TiO_2$/HPMo nanoparticles are indexed to P-O (in the central $PO_4$ tetrahedron) and terminal Mo = O in the $MoO_6$ octahedron, respectively. The characteristic peak at 864 $cm^{-1}$ is weak and the peak at 779 $cm^{-1}$ disappears due to overlapping by peaks attributed to the Ti-O stretching frequency of $TiO_2$. The characteristic peaks at 931, 864, and 594.05 $cm^{-1}$ correspond to terminal Mo = O in the $MoO_6$ octahedron, Mo-$O_b$-Mo ($O_b$: corner-sharing oxygen), and the δ(P-O) vibration, respectively, suggesting that the Keggin structure remained in the ZnO/HPMo nanoparticles (Javidi et al. 2014; Rafiee and Nobakht 2015; Ayati et al. 2016; Wang et al. 2015). Peaks at

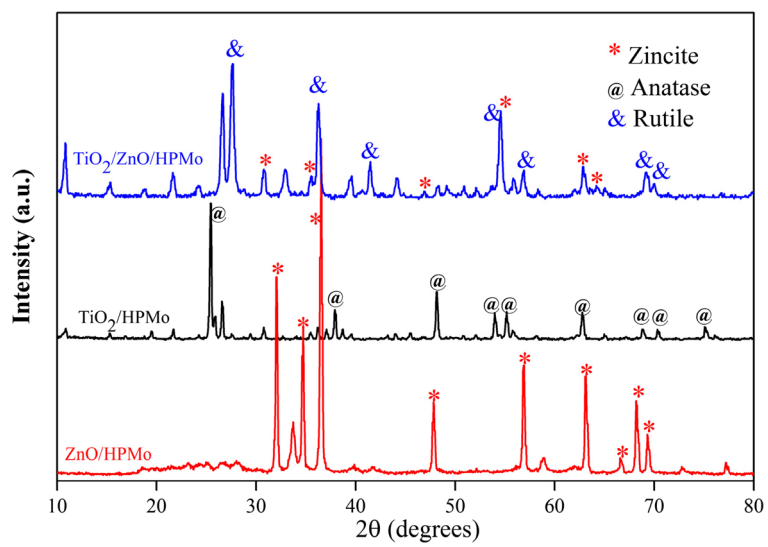


**Fig. 4** XRD patterns of the $TiO_2$/HPMo, ZnO/HPMo, and $TiO_2$/ZnO/HPMo nanoparticles

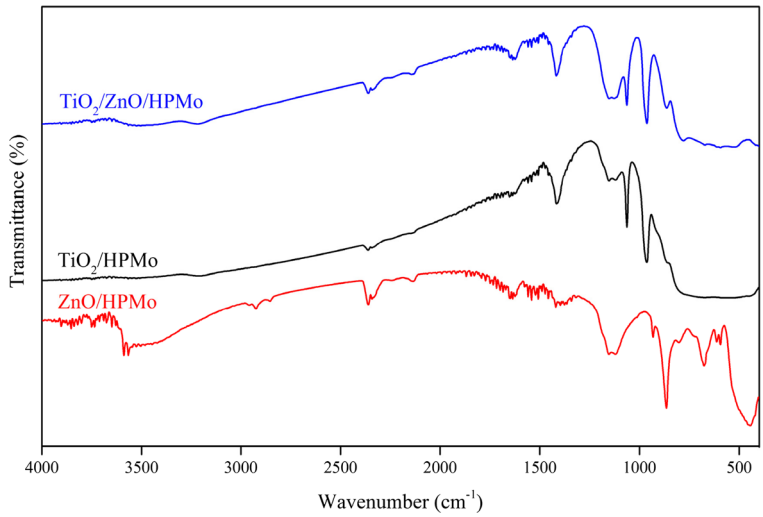


**Fig. 5** The FT-IR absorption spectrum of the $TiO_2$/HPMo, ZnO/HPMo, and $TiO_2$/ZnO/HPMo nanoparticles

1062, 962, 864, and 779 $cm^{-1}$ (Mo-$O_c$-Mo) also indicate the remainder of the Keggin structure in the $TiO_2$/ZnO/HPMo nanoparticles.

*Optical properties*

UV-Vis absorption spectra of nanoparticles are shown in Fig. 6. As can be seen, heterogenization of phosphomolybdic acid on $TiO_2$ and ZnO nanoparticles improves light absorption of nanoparticles and shifts the absorption edge of $TiO_2$ and ZnO from the UV to the visible region. $TiO_2$ is a material of indirect transition and ZnO is considered an n-type direct bandgap semiconductor (Kwiatkowski et al. 2015). Mixing the nanoparticles with direct and indirect transition would be rather problematic. Since it is unclear which one we should use for measuring optical band gap, we decided to assume that $TiO_2$/ZnO/HPMo allows transition both directly (Fig. 6c) and indirectly (Fig. 6b). The band gap of $TiO_2$ and ZnO nanoparticles (Fig. 6b, c) decreases in nanocomposites. The estimated band gaps of $TiO_2$/HPMo, ZnO/HPMo, and $TiO_2$/ZnO/HPMo (indirect and direct transition) are 3.02, 3.1, 2.74, and 2.89, respectively. The shift of the absorption band toward the visible range for $TiO_2$ might be due to doping with heteropoly acids and the rare earth ions (Shi et al. 2012).

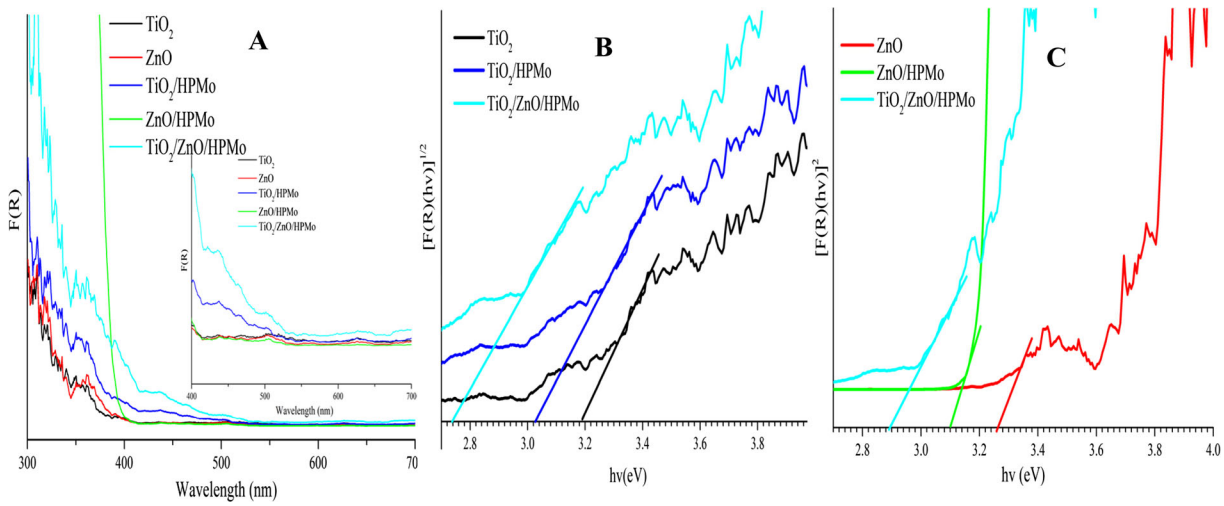


**Fig. 6** Kubelka-Munk curves of nanoparticles (**a**) and band gap determination for indirect transition (**b**) and direct transition (**c**)

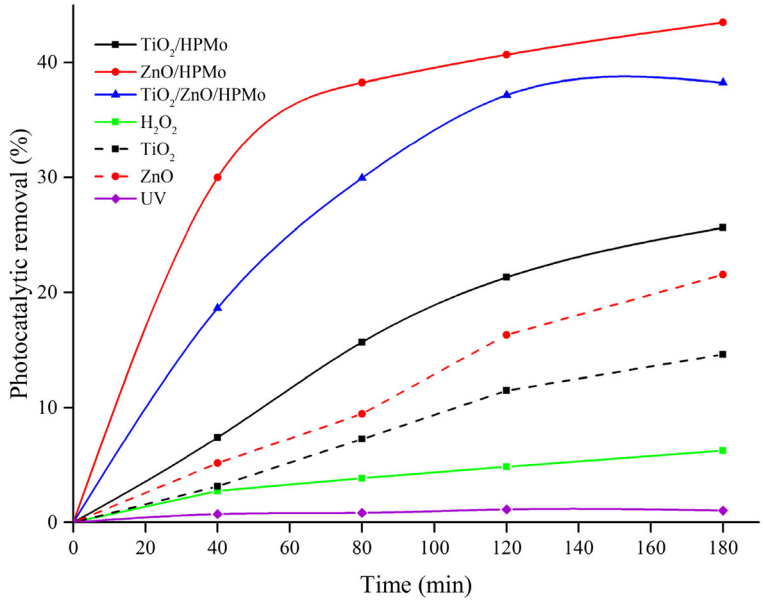


**Fig. 7** The aniline degradation using synthesized nanoparticles

(Yang et al. 2008) also reported that combining $H_3PW_{12}O_{40}$ with $TiO_2$/float pearls could improve absorption intensity of $TiO_2$/float pearls in UV region.

*Photocatalytic activity*

Photocatalytic activity of synthesized nanoparticles toward aniline degradation is presented in Fig. 7. Photocatalytic removal of aniline achieved by $TiO_2$/HPMo, ZnO/HPMo, and $TiO_2$/ZnO/HPMo was about 26, 45, and 38% in 180 min, respectively. On the other hand, only 14, 21, and 6% of aniline was degraded by $TiO_2$, ZnO, and $H_2O_2$ at the same contact time, respectively. The photocatalytic degradation activity of composite nanoparticles remarkably increased as a result of combination with $H_3PMo_{12}O_{40}$ compared to $TiO_2$ and ZnO nanoparticles. Hydrogen peroxide as an electron acceptor reacts with the conduction band electrons. Therefore, it prevents recombination of electron-hole pairs. Consequently, the generation of hydroxyl radicals will

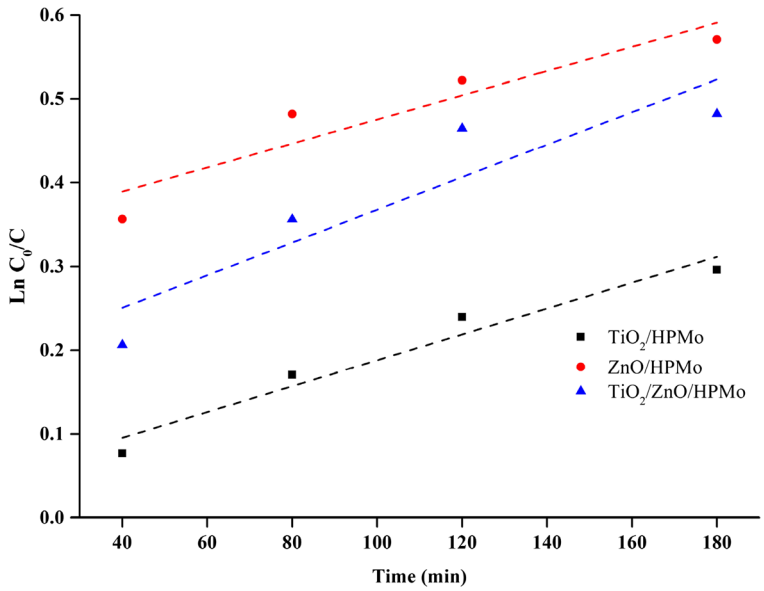


**Fig. 8** The degradation kinetic of aniline using synthesized nanoparticles

increase through the interaction of the photogenerated holes on semiconductor and the adsorbed water and hydroxyl ions. This phenomenon can be shown as follows (Koltsakidou et al. 2017):

$$H_2O_2 + e_{CB}^- \rightarrow {}^{\cdot}OH + HO^- \quad (6)$$

Using Fig. 7, it can be inferred that the photocatalytic activity of synthesized nanoparticles is reduced in the order of ZnO/HPMo > $TiO_2$/ZnO/HPMo > $TiO_2$/HPMo. This order is consistent with the order of light absorption intensity by nanoparticles. The band gap value of ZnO/HPMo is relatively higher than that of $TiO_2$/ZnO/HPMo, but ZnO/HPMo nanoparticle showed higher light absorption intensity around 390 nm. ZnO/HPMo and $TiO_2$/ZnO/HPMo nanoparticles have smaller particle compared with $TiO_2$/HPMo nanoparticles, which provide a higher available surface area for reactions.

Based on these results, there was a significant difference in aniline removal by nanocomposites ($P$ value < 0.001). Results of the post hoc analysis by LSD test confirmed that there is a significant difference in degradation efficiency between all nanoparticles. According to results, combination of POM with nanoparticles also had a statistically significant effect on improve of photocatalytic activity of bare nanoparticles ($P$ value < 0.001).

### *Photocatalytic degradation kinetic*

The Langmuir-Hinshelwood equation is widely applied to explain the kinetics of the heterogeneous photocatalytic process. The plot of Ln($C_0$/C) versus irradiation time is shown in Fig. 8. The kinetic parameters of photocatalytic degradation of aniline are presented in Table 1. Based on the coefficient of determinations presented in Table 1, the results demonstrate a good fit to the Langmuir-Hinshelwood kinetic model, which is in agreement with the results presented in (Huang et al. 2017). The minimum and maximum constant rates belong to ZnO/HPMo (0.0014 $min^{-1}$) and $TiO_2$/ZnO/HPMo (0.0019 $min^{-1}$), respectively. Nivea et al. (Nivea et al. 2014) also reported a constant rate (k) of 0.065 and 0.021 $m^{-1}$ for degradation of methylene blue dye by $TiO_2/H_3PW_{12}O_{40}$ and $TiO_2/H_3PMo_{12}O_{40}$, respectively.

**Table 1** Photocatalytic degradation rate constants (k) of aniline using synthesized nanoparticles

| Parameter | $TiO_2$/HPMo | ZnO/HPMo | $TiO_2$/ZnO/HPMo |
|---|---|---|---|
| k($min^{-1}$)× $10^{-2}$ | 0.15 | 0.14 | 0.19 |
| $R^2$ | 0.955 | 0.879 | 0.838 |

## Conclusion

$TiO_2$/ZnO-supported $H_3PMo_{12}O_{40}$ nanoparticles were synthesized using impregnation method for the first time and their photocatalytic activity under UV-LED light and degradation kinetics as an organic pollutant model were investigated. The results showed that the heterogenization of phosphomolybdic acid on $TiO_2$ and ZnO nanoparticles improves light absorption of nanoparticles and shifts the absorption edge of $TiO_2$ and ZnO from the UV to near the visible region. The band gaps of $TiO_2$ and ZnO nanoparticles were decreased in nanocomposites. The photocatalytic degradation activity of composite nanoparticles remarkably increased as a result of combination with phosphomolybdic acid compared to $TiO_2$ and ZnO nanoparticles. The results also showed a good fit of the obtained data to the Langmuir-Hinshelwood kinetic model.

## References

Anotai, J., Jevprasesphant, A., Lin, Y.-M., & Lu, M.-C. (2012). Oxidation of aniline by titanium dioxide activated with visible light. *Separation and Purification Technology, 84*, 132–137.

Ayati, A., Heravi, M. M., Daraie, M., Tanhaei, B., Bamoharram, F. F., & Sillanpaa, M. (2016). $H_3PMo_{12}O_{40}$ immobilized chitosan/$Fe_3O_4$ as a novel efficient, green and recyclable nanocatalyst in the synthesis of pyrano-pyrazole derivatives. *Journal of the Iranian Chemical Society, 13*(12), 2301–2308.

Choudhury, B., Dey, M., & Choudhury, A. (2013). Defect generation, d-d transition, and band gap reduction in Cu-doped $TiO_2$ nanoparticles. *International Nano Letters, 3*(1), 25.

Eslami, H., Ehrampoush, M. H., Falahzadeh, H., Hematabadi, P. T., Khosravi, R., Dalvand, A., et al. (2018). Biodegradation and nutrients removal from greywater by an integrated fixed-film activated sludge (IFAS) in different organic loadings rates. *AMB Express, 8*(1), 3. https://doi.org/10.1186/s13568-017-0532-9.

Feng, C., Shang, H., & Liu, X. (2014). Photocatalysis of dinitrotoluene decomposition by $H_3PW_{12}O_{40}/TiO_2$ and $H_4SiW_{12}O_{40}/TiO_2$ prepared by a modified sol-gel synthesis and solvothermal treatment method. *Chinese Journal of Catalysis, 35*(2), 168–174.

Huang, Q., Zhang, J., He, Z., Shi, P., Qin, X., & Yao, W. (2017). Direct fabrication of lamellar self-supporting $Co_3O_4$/N/C peroxymonosulfate activation catalysts for effective aniline degradation. *Chemical Engineering Journal, 313*, 1088–1098.

Jamali, A., Vanraes, R., Hanselaer, P., & Van Gerven, T. (2013). A batch LED reactor for the photocatalytic degradation of phenol. *Chemical Engineering and Processing: Process Intensification, 71*, 43–50.

Javidi, J., Esmaeilpour, M., Rahiminezhad, Z., & Dodeji, F. N. (2014). Synthesis and characterization of $H_3PW_{12}O_{40}$ and $H_3PMo_{12}O_{40}$ nanoparticles by a simple method. *Journal of Cluster Science, 25*(6), 1511–1524.

Khosravi, R., Eslami, H., Almodaresi, S. A., Heidari, M., Fallahzadeh, R. A., Taghavi, M., et al. (2017). Use of geographic information system and water quality index to assess groundwater quality for drinking purpose in Birjand City, Iran. *Desalination and Water Treatment, 67*, 74–83.

Koltsakidou, A., Antonopoulou, M., Evgenidou, E., Konstantinou, I., Giannakas, A., Papadaki, M., et al. (2017). Photocatalytical removal of fluorouracil using $TiO_2$-P25 and N/S doped $TiO_2$ catalysts: a kinetic and mechanistic study. *Science of the Total Environment, 578*, 257–267.

Ku, Y., Chiu, P.-C., & Chou, Y.-C. (2010). Decomposition of aniline in aqueous solution by UV/$TiO_2$ process with applying bias potential. *Journal of Hazardous Materials, 183*(1), 16–21.

Kumari, R., Sahai, A., & Goswami, N. (2015). Effect of nitrogen doping on structural and optical properties of ZnO nanoparticles. *Progress in Natural Science: Materials International, 25*(4), 300–309.

Kuvarega, A. T., Krause, R. W., & Mamba, B. B. (2015). Evaluation of the simulated solar light photocatalytic activity of N, Ir co-doped $TiO_2$ for organic dye removal from water. *Applied Surface Science, 329*, 127–136.

Kwiatkowski, M., Bezverkhyy, I., & Skompska, M. (2015). ZnO nanorods covered with a $TiO_2$ layer: simple sol–gel preparation, and optical, photocatalytic and photoelectrochemical properties. *Journal of Materials Chemistry A, 3*(24), 12748–12760.

Leong, K. H., Monash, P., Ibrahim, S., & Saravanan, P. (2014). Solar photocatalytic activity of anatase $TiO_2$ nanocrystals synthesized by non-hydrolitic sol–gel method. *Solar Energy, 101*, 321–332.

Li, N., Vorontsov, A., & Jing, L. (2015). Physicochemical properties and photocatalytic activity of $H_3PW_{12}O_{40}/TiO_2$. *Kinetics and Catalysis, 56*(3), 308–315.

López, R., & Gómez, R. (2012). Band-gap energy estimation from diffuse reflectance measurements on sol–gel and commercial $TiO_2$: a comparative study. *Journal of Sol-Gel Science and Technology, 61*(1), 1–7.

Lu, N., Lu, Y., Liu, F., Zhao, K., Yuan, X., Zhao, Y., et al. (2013). $H_3PW_{12}O_{40}/TiO_2$ catalyst-induced photodegradation of bisphenol A (BPA): kinetics, toxicity and degradation pathways. *Chemosphere, 91*(9), 1266–1272.

Natarajan, T. S., Thomas, M., Natarajan, K., Bajaj, H. C., & Tayade, R. J. (2011). Study on UV-LED/$TiO_2$ process for degradation of Rhodamine B dye. *Chemical Engineering Journal, 169*(1), 126–134.

Nivea, R., Gunasekaran, V., Kannan, R., Sakthivel, T., & Govindan, K. (2014). Enhanced photocatalytic efficacy of hetropolyacid pillared $TiO_2$ nanocomposites. *Journal of Nanoscience and Nanotechnology, 14*(6), 4383–4386.

Norwitz, G., & Keliher, P. N. (1981). Spectrophotometric determination of aniline by the diazotization-coupling method with N-(1-naphthyl) ethylenediamine as the coupling agent. *Analytical Chemistry, 53*(8), 1238–1240.

Orge, C., Faria, J., & Pereira, M. (2016). Photocatalytic ozonation of aniline with $TiO_2$-carbon composite materials. Journal of Environmental Management*, In press*.

Rafiee, E., & Nobakht, N. (2015). Keggin type heteropoly acid, encapsulated in metal-organic framework: A heterogeneous and recyclable nanocatalyst for selective oxidation of sulfides and deep desulfurization of model fuels. *Journal of Molecular Catalysis A: Chemical, 398*, 17–25.

Samarghandy, M. R., Hoseinzade, E., Taghavi, M., & Hoseinzadeh, S. (2011). Biosorption of Reactive Black 5 from aqueous solution using acid-treated biomass from potato peel waste. *BioResources, 6*(4), 4840–4855.

Sarwade, V., & Gawai, K. (2014). Biodegradation of aniline by alkaliphilic strain Bacillus badius D1. *IOSR Journal of Environmental Science, Toxicology and Food Technology, 8*(5), 71–78.

Shi, H., Zhang, T., An, T., Li, B., & Wang, X. (2012). Enhancement of photocatalytic activity of nano-scale $TiO_2$ particles co-doped by rare earth elements and heteropolyacids. *Journal of Colloid and Interface Science, 380*(1), 121–127.

Sun, L., Li, Y., & Li, A. (2015). Treatment of actual chemical wastewater by a heterogeneous fenton process using natural pyrite. *International Journal of Environmental Research and Public Health, 12*(11), 13762–13778.

Szczepanik, B., & Słomkiewicz, P. (2016). Photodegradation of aniline in water in the presence of chemically activated halloysite. *Applied Clay Science, 124*, 31–38.

Taghavi, M., Tabatabaee, M., Ehrampoush, M. H., Ghaneian, M. T., Afsharnia, M., Alami, A., et al. (2018). Synthesis, characterization and photocatalytic activity of $TiO_2$/ZnO-supported phosphomolybdic acid nanocomposites. *Journal of Molecular Liquids, 249*, 546–553.

Taghi Ghaneian, M., Ebrahimi, A., Salimi, J., Khosravi, R., Fallahzadeh, R. A., Amrollahi, M., et al. (2016). Photocatalytic degradation of 2, 4-dichlorophenoxyacetic acid from aqueous solutions using $In_2O_3$ nanoparticles. *Journal of Mazandaran University of Medical Sciences, 26*(137), 159–170.

Toyoura, K., Tsujimura, H., Goto, T., Hachiya, K., Hagiwara, R., & Ito, Y. (2005). Optical properties of zinc nitride formed by molten salt electrochemical process. *Thin Solid Films, 492*(1), 88–92.

Wang, W., Huang, Y., & Yang, S. (2010). Photocatalytic degradation of nitrobenzene wastewater with $H_3PW_{12}O_{40}/TiO_2$. In *Mechanic Automation and Control Engineering (MACE), 2010 International Conference on,* IEEE (pp. 1303–1305).

Wang, S., Tang, R., Zhang, Y., Chen, T., & Wang, G. (2015). 12-Molybdophosphoric acid supported on titania: a highly active and selective heterogeneous catalyst for the transesterification of dimethyl carbonate and phenol. *Chemical Engineering Science, 138*, 93–98.

Wei, G., Zhang, L., Wei, T., Luo, Q., & Tong, Z. (2012). UV–$H_2O_2$ degradation of methyl orange catalysed by $H_3PW_{12}O_{40}$/activated clay. *Environmental Technology, 33*(14), 1589–1595.

Xu, L., Wang, G., Ma, F., Zhao, Y., Lu, N., Guo, Y., et al. (2012). Photocatalytic degradation of an aqueous sulfamethoxazole over the metallic silver and Keggin unit codoped titania

nanocomposites. *Applied Surface Science, 258*(18), 7039–7046.

Xu, L., Zang, H., Zhang, Q., Chen, Y., Wei, Y., Yan, J., et al. (2013). Photocatalytic degradation of atrazine by $H_3PW_{12}O_{40}$/Ag–$TiO_2$: kinetics, mechanism and degradation pathways. *Chemical Engineering Journal, 232*, 174–182.

Yang, W., Gao, H., Li, S., Yan, Y., Huo, P., & Yao, W. (2008). Preparation of floatable compound photocatalyst of phosphotungstic acid/titanium dioxide/float pearls and its degradation capability to wastewater of dye. In *Bioinformatics and Biomedical Engineering. ICBBE 2008. The 2nd International Conference on, 2008* (pp. 2892–2895): IEEE.

Yang, S., Huang, Y., Wang, Y., Yang, Y., Xu, M., & Wang, G. (2012). Photocatalytic degradation of Rhodamine B with H3PW12O40/SiO2 sensitized by H2O2. *International Journal of Photoenergy, 2012*.

Zabihi-Mobarakeh, H., & Nezamzadeh-Ejhieh, A. (2015). Application of supported $TiO_2$ onto Iranian clinoptilolite nanoparticles in the photodegradation of mixture of aniline and 2, 4-dinitroaniline aqueous solution. *Journal of Industrial and Engineering Chemistry, 26*, 315–321.